batteries

MDPI

Article

An Evaluation Modeling Study of Thermal Runaway in Li-Ion Batteries Based on Operation Environments in an Energy Storage System

Min-Haeng Lee, Sung-Moon Choi, Kyung-Hwa Kim, Hyun-Sang You, Se-Jin Kim and Dae-Seok Rho *

Department of Electrical Engineering, Korea University of Technology & Education (KUT), Cheonan-si 31253, Republic of Korea; dlalsgod97@koreatech.ac.kr (M.-H.L.); moon9507@koreatech.ac.kr (S.-M.C.); kyunghwa316@koreatech.ac.kr (K.-H.K.); hsyu@koreatech.ac.kr (H.-S.Y.); tpwls1578@koreatech.ac.kr (S.-J.K.)
* Correspondence: dsrho@koreatech.ac.kr; Tel.: +82-41-560-1167

Abstract: According to the green growth and carbon-neutral policy in Korea, the installation of large-capacity ESSs is rapidly being increased, but a total number of 50 ESS fire cases have occurred since the end of 2023. ESSs are typically composed of series-parallel connections with numerous Li-ion batteries, and when the temperature of a deteriorated cell increases due to thermal, electrical, and mechanical stress, thermal runaway can occur due to additional heat generated by an internal chemical reaction. Here, an internal chemical reaction in a Li-ion battery results in the different characteristics on the decomposition reaction and heat release depending on the operation conditions in the ESS, such as the rising temperature rate, convective heat transfer coefficient, and C-rate of charging and discharging. Therefore, this paper presents mathematical equations and modeling of thermal runaway, composed of the heating device section, heat release section by chemical reaction, chemical reaction section at the SEI layer, chemical reaction section between the negative and positive electrodes and solvents, and chemical reaction section at the electrolyte by itself, based on MATLAB/SIMULINK (2022), which were validated by a thermal runaway test device. From the simulation and test results based on the proposed simulation modeling and test device according to the operation conditions in ESSs, it was found that the proposed modeling is an effective and reliable tool to evaluate the processing characteristics of thermal runaway because the occurrence time intervals and maximum temperatures had almost the same values in both the test device and simulation modeling. Accordingly, it was confirmed that the rising temperature rate and the convective heat transfer coefficient were more critical in the thermal runaway than the C-rate of charging and discharging.

Keywords: Li-ion battery; thermal runaway; operation environment; mathematical equation; evaluation modeling; MATLAB/SIMULINK

Citation: Lee, M.-H.; Choi, S.-M.; Kim, K.-H.; You, H.-S.; Kim, S.-J.; Rho, D.-S. An Evaluation Modeling Study of Thermal Runaway in Li-Ion Batteries Based on Operation Environments in an Energy Storage System. *Batteries* **2024**, *10*, 332. https://doi.org/10.3390/batteries10090332

Academic Editors: Fei Feng, Rui Ling, Yi Xie, Shunli Wang, Jinhao Meng, Jiale Xie and Zhenbo Wang

Received: 20 June 2024
Revised: 2 August 2024
Accepted: 13 September 2024
Published: 19 September 2024

1. Introduction

Recently, the installation of large-capacity energy storage systems (ESSs) in South Korea have been rapidly increased to carry out various functions such as power stabilization of renewable energy sources, demand response, and frequency regulation, but the fire cases in ESSs have continuously occurred since August 2017 [1–3]. From the analysis results of 40 fire accident cases occurring from the end of 2022 based on the operation environments such as installation location, building type, and application, it is known that the fire accident rate in ESSs for renewable energy sources is much higher than other applications because they are installed and operate in relatively poor conditions [4,5]. On the other hand, ESSs are composed of series-parallel connections with a number of Li-ion batteries, and when the temperature of a deteriorated cell increases in a continuous way due to thermal, electrical, and mechanical stresses, a thermal runaway phenomenon can occur according to the additional heat generated by an internal chemical reaction [6–8]. Therefore, this paper formulated mathematical equations of thermal runaway in Li-ion batteries and

then performed its evaluation modeling using MATLAB/SIMULINK (2022) S/W, which consists of a heating device section, a heat release section by chemical reaction, a chemical reaction section at the solid electrolyte interphase (SEI) layer, a chemical reaction section between negative and positive electrodes and solvents, and a chemical reaction section at the electrolyte by itself. Also, this paper implemented a test device for thermal runaway, which is composed of a heating chamber section, a heating device section, and a monitoring and control section in order to validate the effectiveness of the proposed modeling. From the simulation and test results based on the proposed simulation modeling and test device according to the operation conditions in ESSs, it is confirmed that the proposed modeling is an effective and reliable tool to evaluate the processing characteristics of thermal runaway because the occurrence time intervals and maximum temperatures in the test device are nearly identical to the results of simulation modeling. Also, it is found that as the convective heat transfer coefficient becomes higher due to the humidity and ventilation condition inside the battery module, the thermal runaway is occurs within a short time interval, and then the thermal runaway from a single cell can easily propagate to adjacent cells depending on the convective heat transfer coefficients. Based on the operation conditions in ESSs, it is clear that the rising temperature rate and the convective heat transfer coefficient are more critical in the thermal runaway than the C-rate of charging and discharging.

2. Mathematical Equations of Thermal Runaway in Li-Ion Batteries for ESSs

In order to evaluate the processing characteristics of thermal runaway in Li-ion batteries, this paper assumes that the temperature of a battery is raised by a heating chamber based on UL9450A, being one of the test methods shown in reference [9]. Here, the heat flux through the air in heating chamber is calculated by the convective heat transfer coefficient and the temperature difference between the heating device and battery, as shown in Equation (1) according to Newton's law of cooling. Also, the temperature variation in the battery due to the heating can be formulated as shown in Equation (2) by considering the heat flux and cross area, volume, density, and specific heat capacity of the current collectors in positive and negative electrodes [10,11].

$$q''(t) = k_{conv} \cdot (C_{heat} - C_{batt}(t)) \tag{1}$$

$$\Delta C_{batt,heat}(t) = \int_0^t \frac{2 \cdot D \cdot q''(t)}{v \cdot \rho_{batt} \cdot S_{heat}} dt \tag{2}$$

where q'' is the heat flux to the battery, k_{conv} is the convective heat transfer coefficient, C_{heat} is the temperature of the heating device, C_{batt} is the temperature of the battery, $\Delta C_{batt,heat}$ is the temperature variation in the battery due to heating, D is the cross area of the current collector in the battery, v is the volume of the current collector in the battery, ρ_{batt} is the density of the current collector in the battery, and S_{heat} is the specific heat capacity of the current collector in the battery.

Furthermore, the total heat release by internal chemical reactions occurring in a Li-ion battery can be expressed as shown in Equation (3), and the temperature variation in a battery due to chemical reactions is calculated as shown in Equation (4) [12–14].

$$Q_{total}(t) = Q_{sei} + Q_{nega} + Q_{posi} + Q_{elect} \tag{3}$$

$$\Delta C_{batt,chem}(t) = \int_0^t \frac{Q_{total}(t)}{\rho_{batt} \cdot S_{heat}} dt \tag{4}$$

where Q_{total} is the total heat release by internal chemical reactions, Q_{sei} is the heat release by the decomposition of the SEI layer, Q_{nega} is the heat release between the negative electrode and the solvent, Q_{posi} is the heat release between the positive electrode and the solvent, Q_{elect} is the heat release by the decomposition of the electrolyte, $\Delta C_{batt,chem}$ is the temperature variation in the battery due to the chemical reaction.

The heat release by the decomposition of the SEI layer can be formulated as shown in Equation (3), and the reaction velocity of the decomposition of the SEI layer is calculated as shown in Equations (4) and (5) according to the thermal decomposition reaction equation of a solid component based on the Arrhenius equation [15–17].

$$Q_{sei}(t) = H_{sei} \cdot \rho_c \cdot V_{sei}(t) \tag{5}$$

$$V_{sei}(t) = A_{sei} \cdot M_{sei}(t) \cdot exp^{\left(-\frac{e_{sei}}{R \cdot C_{batt}}\right)} \tag{6}$$

$$\frac{dM_{sei}(t)}{dt} = -V_{sei}(t) \tag{7}$$

where H_{sei} is the reaction heat by decomposition of the SEI layer, ρ_c is the volume-specific carbon content in the SEI layer, V_{sei} is the reaction velocity of the decomposition of the SEI layer, A_{sei} is the frequency factor of the decomposition of the SEI layer, e_{sei} is the activation energy of the decomposition of the SEI layer, R is the universal gas constant, and M_{sei} is the dimensionless amount of lithium-containing meta-stable species in the SEI layer.

In addition, the heat release between the negative electrode and solvent, which is a one-dimensional diffusion type, can be expressed as shown in Equation (8), and the reaction velocity between the negative electrode and solvent is calculated as shown in Equation (9). As the chemical reaction is continuously processed, the concentration of lithium in the negative electrode is decreased according to Equation (10), and the thickness of the SEI layer is increased based on Equation (11) due to the formation of the SEI layer.

$$Q_{nega}(t) = H_{nega} \cdot \rho_c \cdot V_{nega}(t) \tag{8}$$

$$V_{nega}(t) = -A_{nega} \cdot M_{nega}(t) \cdot exp^{\left(-\frac{W_{sei}(t)}{W_{sei}(0)}\right)} \cdot exp^{\left(-\frac{e_{nega}}{R \cdot C_{batt}}\right)} \tag{9}$$

$$\frac{dW_{sei}(t)}{dt} = V_{nega}(t) \tag{10}$$

$$\frac{dM_{nega}(t)}{dt} = -V_{nega}(t) \tag{11}$$

where H_{nega} is the reaction heat between the negative electrode and solvent, V_{nega} is the reaction velocity between the negative electrode and solvent, A_{nega} is the frequency factor between the negative electrode and solvent, W_{sei} is the thickness of the SEI layer, e_{nega} is the activation energy between the negative electrode and the solvent, and M_{nega} is the dimensionless amount of lithium within the carbon.

Also, the heat release between the positive electrode and solvent, which is an autocatalytic reaction, can be formulated as shown in Equation (12), and the reaction velocity between the positive electrode and solvent is calculated as shown in Equations (13) and (14).

$$Q_{posi}(t) = H_{posi} \cdot \rho_{posi} \cdot V_{posi}(t) \tag{12}$$

$$V_{posi}(t) = A_{posi} \cdot \alpha(t) \cdot (1 - \alpha(t)) \cdot exp^{\left(-\frac{e_{posi}}{R \cdot C_{batt}}\right)} \tag{13}$$

$$\frac{d\alpha(t)}{dt} = V_{posi}(t) \tag{14}$$

where H_{posi} is the reaction heat between the positive electrode and the solvent, ρ_{posi} is the volume-specific positive active content, V_{posi} is the reaction velocity between the positive electrode and the solvent, A_{posi} is the frequency factor between the positive electrode and the solvent, e_{posi} is the activation energy between the positive electrode and the solvent, and α is the conversion rate.

On the other hand, the heat release by decomposition of the electrolyte, which is a one-dimensional diffusion type, can be expressed as shown in Equation (15), and the reaction velocity of the decomposition of the electrolyte is calculated as shown in Equations (16) and (17).

$$Q_{elect}(t) = H_{elect} \cdot \rho_{elect} \cdot V_{elect}(t) \tag{15}$$

$$V_{elect}(t) = A_{elect} \cdot M_{elect}(t) \cdot exp^{\left(-\frac{e_{elect}}{R \cdot C_{batt}}\right)} \tag{16}$$

$$\frac{dM_{elect}(t)}{dt} = -V_{elect}(t) \tag{17}$$

where H_{elect} is the reaction heat by the decomposition of the electrolyte, ρ_{elect} is the volume-specific electrolyte active content, V_{elect} is the reaction velocity of the decomposition of the electrolyte, A_{elect} is the frequency factor of the decomposition of the electrolyte, e_{elect} is the activation energy of the decomposition of the electrolyte, and M_{elect} is the dimensionless concentration of the electrolyte.

Finally, this paper adapted the concept of a new single particle (SP) model found in reference [18] that includes electrolyte physics and a stress–diffusion coupling effect to describe the charging and discharging operation. Here, the analytical equations for electrolyte potential are derived based on the electrolyte charge conservation equation, and the stress-enhanced diffusion is coupled with electrochemical physics inside the entire battery [19,20]. Based on this concept, this paper presents the modeling of heat generation due to ohmic heat according to C-rate of charging and discharging by using the electrochemical–thermal coupled model as shown in reference [21].

3. Evaluation Modeling of Thermal Runaway Using MATLAB/SIMULINK S/W

Based on the proposed mathematical equations, the modeling of the heating device section can be expressed using MATLAB/SIMULINK, as shown in Figure 1. Here, Figure 1a shows the heat flux to the battery, which is created by Equation (1), and Figure 1b shows the temperature variation in the battery due to the heating, which is created by Equation (2).

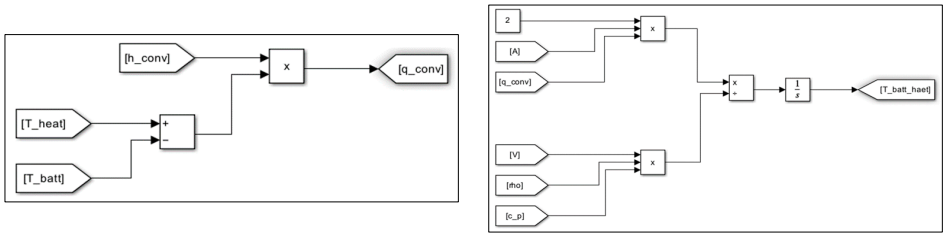

(**a**) (**b**)

Figure 1. Modeling of the heating device section for the battery: (**a**) heat flux to the battery; (**b**) temperature variation in the battery due to heating.

Also, the modeling of the heat release section by chemical reaction in a Li-ion battery can be illustrated as shown in Figure 2. Here, Figure 2a shows the total heat release by an internal chemical reaction, which is designed by Equation (3), and Figure 2b is the temperature variation of a battery due to internal chemical reactions, which is designed by Equation (4).

Furthermore, the modeling of the chemical reaction section at the SEI layer can be demonstrated as shown in Figure 3. Here, Figure 3a shows the modeling of heat release by the decomposition of the SEI layer, which is created by Equation (5), and Figure 3b is the reaction velocity of the decomposition of the SEI layer, which is created by Equations (6) and (7).

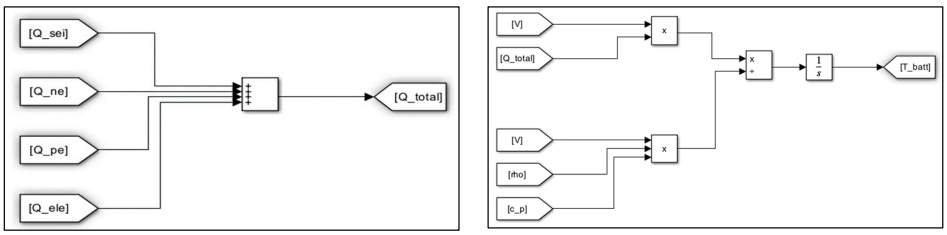

(**a**) (**b**)

Figure 2. Modeling of the heat release section by chemical reaction in a battery: (**a**) total heat release by internal chemical reactions; (**b**) temperature variation in the battery due to chemical reaction.

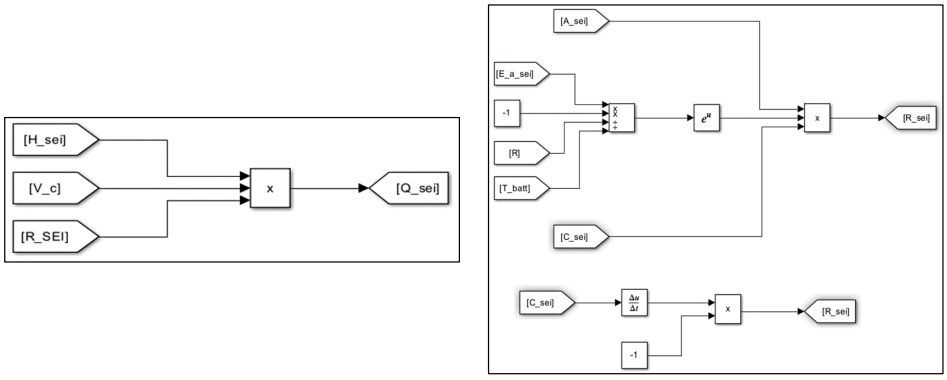

(**a**) (**b**)

Figure 3. Modeling of the chemical reaction section at the SEI layer: (**a**) heat release by the decomposition of the SEI layer; (**b**) reaction velocity of the decomposition of the SEI layer.

In addition, the chemical reaction section between the negative electrode and solvent can be expressed as shown in Figure 4. Here, Figure 4a shows the heat release between the negative electrode and the solvent, which is designed by Equation (8), and Figure 4b is the reaction velocity between the negative electrode and the solvent, which is designed by Equations (9)–(11). Also, the chemical reaction section between the positive electrode and solvent can be illustrated according to Equations (12)–(14) in the same way.

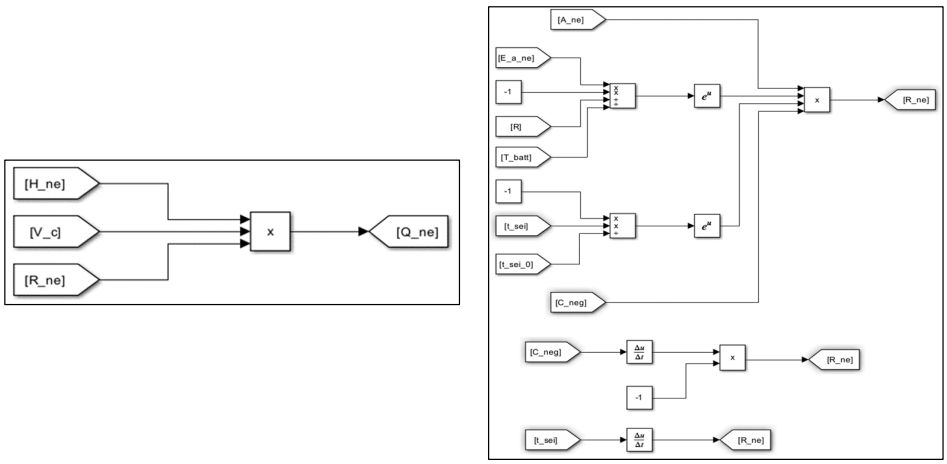

(**a**) (**b**)

Figure 4. Modeling of the chemical reaction section between the negative electrode and the solvent: (**a**) heat release between the negative electrode and the solvent; (**b**) reaction velocity between the negative electrode and the solvent.

Finally, the modeling of the chemical reaction section at the electrolyte by itself can be demonstrated as shown in Figure 5. Here, Figure 5a shows the heat release by the decomposition of the electrolyte, which is created by Equation (15), and Figure 5b is the reaction velocity of the decomposition of the electrolyte, which is created by Equations (16) and (17).

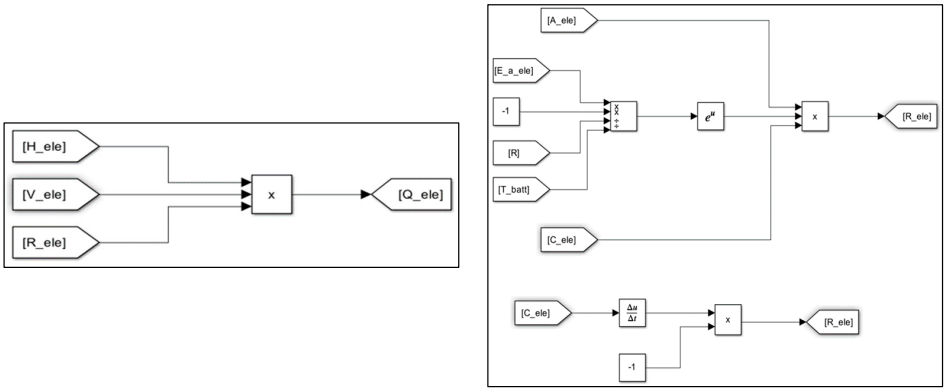

(**a**) (**b**)

Figure 5. Modeling of the chemical reaction section at the electrolyte: (**a**) heat release by the decomposition of the electrolyte; (**b**) reaction velocity of the decomposition of the electrolyte.

4. Implementation of a Test Device for Thermal Runaway in a Li-Ion Battery

In order to validate the proposed modeling, this paper designed and implemented the test device for thermal runaway in a Li-ion battery, which consists of a heating chamber section, a heating device section, and a monitoring and control section, and we evaluated the processing characteristics of thermal runaway due to external heating [22]. Here, the heating chamber section was assembled with reinforced steel frames to withstand thermal runaway, and a transparent polycarbonate window was installed on the front door to check the test processing. Also, the heating device and control sections were composed of a copper pipe, heat wire, and temperature controller, as shown in Figure 6. Here, a cylindrical Li-ion battery was inserted into the copper pipe, which was wrapped with heat wire, and then it was heated through the temperature controller to uniformly raise the temperature of the battery surface. In addition, the temperature of the battery was increased constantly by the RAMP function of the temperature controller, which was regulated accurately through temperature feedback from a thermocouple installed between the battery and copper pipe.

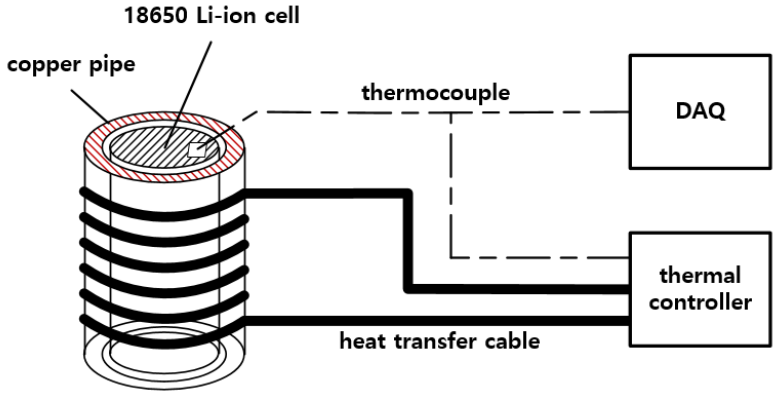

Figure 6. Configuration of the heating device.

Based on the components mentioned earlier, the outline of the implemented test device for thermal runaway in a Li-ion battery is shown in Figure 7. Here, Figure 7a shows the heating chamber section, and Figure 7b is the heating device and control section. Also, the thermal runaway test was performed in the laboratory with forced ventilation,

explosion protection, and fire extinguishing systems to prevent an explosion caused by the flammable gases.

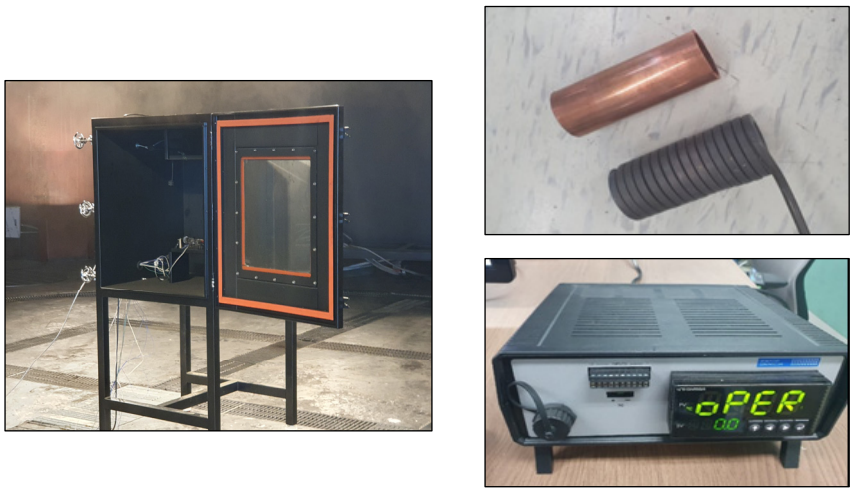

(**a**) (**b**)

Figure 7. Implementation of the test device for thermal runaway: (**a**) outline of the heating chamber section; (**b**) outline of the heating device and control section.

5. Case Studies

5.1. Simulation Conditions

In order to evaluate the processing characteristics of thermal runaway in a Li-ion battery according to operation environments, simulation conditions were assumed as shown in Table 1. Here, the rising temperature rates at the battery surface through the external heating were set as 3, 5, and 7 [°C/min], and the C-rates of charging and discharging were adopted as 0.5 and 5[C]. Also, the internal parameters in the 18650 cylindrical Li-ion battery were assumed as shown in Table 2 [23,24].

Table 1. Simulation conditions.

Items	Contents
Rising temperature rate [°C/min]	3, 5, 7
C-rate of charging and discharging [C]	0.5, 5
Convective heat transfer coefficient [W/(m^2·°C)]	6, 15

Table 2. Parameters of the internal Li-ion battery.

Symbols	Items	Values
R	universal gas constant	8.31
F	Faraday constant	96.485
H_{sei}	reaction heat by decomposition of the SEI layer	2.6×10^5
H_{nega}	reaction heat between the negative electrode and solvent	1.7×10^6
H_{posi}	reaction heat between the positive electrode and solvent	7.9×10^5
H_{elect}	reaction heat by the decomposition of the electrolyte	1.6×10^5
V_c	volume-specific carbon content in the SEI layer	1.7×10^3
V_{posi}	volume-specific positive active content	1.3×10^3
V_{elect}	volume-specific electrolyte active content	5×10^2

Table 2. *Cont.*

Symbols	Items	Values
A_{sei}	frequency factor of the decomposition of the SEI layer	1.7×10^{14}
A_{nega}	frequency factor between the negative electrode and solvent	5.0×10^{12}
A_{posi}	frequency factor between the positive electrode and solvent	2.3×10^{13}
A_{elect}	frequency factor of the decomposition of the electrolyte	5.1×10^{24}
e_{sei}	activation energy of the decomposition of the SEI layer	1.4×10^{5}
e_{nega}	activation energy between the negative electrode and solvent	1.4×10^{5}
e_{posi}	activation energy between the positive electrode and solvent	1.5×10^{5}
e_{elect}	activation energy of the decomposition of the electrolyte	2.7×10^{5}
M_{sei}	dimensionless amount of lithium-containing meta-stable species in the SEI layer	0.15
M_{nega}	dimensionless amount of lithium within the carbon in a negative electrode	0.75
M_{elect}	dimensionless concentration of the electrolyte	1
α	conversion rate	0.04
$W_{sei}(0)$	initial value of W_{sei}	0.033

5.2. Validation of the Proposed Modeling with Rising Temperature Rate

In order to validate the proposed modeling, the processing characteristics of thermal runaway in a Li-ion battery according to the test device and simulation modeling can be compared as shown in Figure 8. Here, the graphs ① and ② in Figure 8 show the thermal runaway results by using the test device and simulation modeling, in the case of the rising temperature rate of 5 [°C] per minute in the battery. Namely, the occurrence time intervals of thermal runaway by the test device and simulation modeling were obtained as 28 min 43 s and 29 min 19 s, respectively, and the maximum temperatures were 798 [°C] and 749.8 [°C]. Therefore, it is confirmed that the proposed modeling is an effective and reliable tool to evaluate the processing characteristics of thermal runaway because the occurrence time intervals and maximum temperatures had almost the same values in both the test device and the simulation modeling.

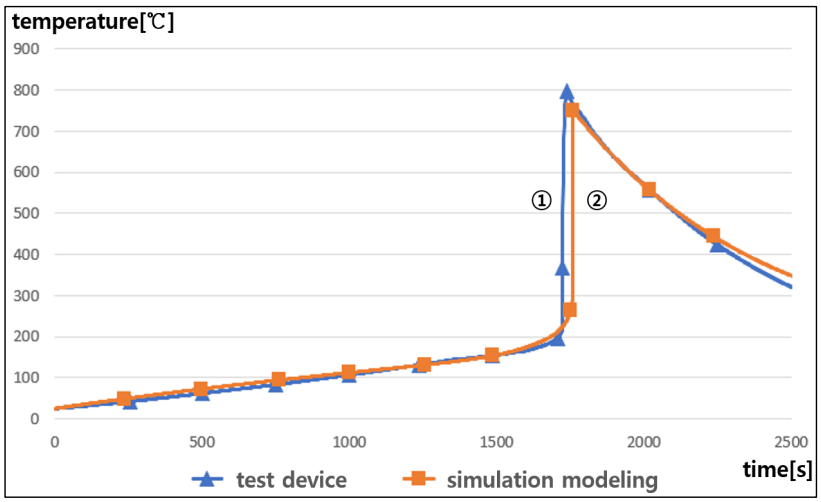

Figure 8. Profile of thermal runaway of the test device and simulation.

5.3. Thermal Runaway Characteristics with Rising Temperature Rate

Based on the simulation conditions mentioned above, the processing characteristics of thermal runaway according to the rising temperature rate were obtained as shown in Figure 9. As shown in the graph ① in Figure 9, when the rising temperature rate in the battery was by 3 [°C] per minute, thermal runaway occurred in about 46 min. Also, if the rising temperature rates were by 5 [°C] and 7 [°C] per minute, the occurrence time intervals of thermal runaway were calculated as 28 min and 20 min, respectively, as shown in the graphs ② and ③ in Figure 9. Comparing the graph ③ with graph ①, the time interval of thermal runaway was shortened by up to 26 min according to the rising temperature rate. Therefore, it was found that as the rising temperature rate became higher, the chemical reaction inside the battery was accelerated and then the occurrence time interval of thermal runaway was shortened.

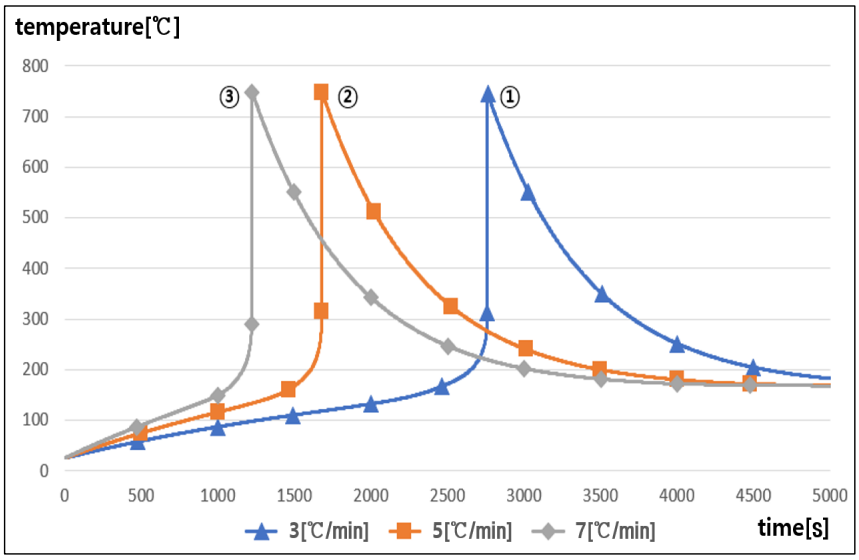

Figure 9. Profile of thermal runaway with the rising temperature rate.

5.4. Thermal Runaway Characteristics with the C-Rate of Charging and Discharging

The processing characteristics of thermal runaway in a Li-ion battery according to the C-rate of charging and discharging were obtained for the rising temperature rate of 5 [°C] per minute, as shown in Figure 10. The graph ① in Figure 10 shows the thermal runaway characteristics in the case of the 0.5 C-rate in charging and discharging, which applies for the test conditions in IEC 62619, and it was found that thermal runaway occurred in 29 min 20 s [25]. On the other hand, the graph ② in Figure 10 shows that the occurrence time interval of thermal runaway was calculated as about 28 min in the case of the 5 C-rate. Comparing the graph ② with graph ①, the time interval of thermal runaway was shortened by up to 80 s depending on the C-rate of charging and discharging. Consequently, it is clear that as the C-rate of charging and discharging became higher, the occurrence time interval of thermal runaway was slightly shortened due to the heat release from the internal resistance in the battery.

5.5. Thermal Runaway Characteristics with the Convective Heat Transfer Coefficient

The processing characteristics of thermal runaway in a Li-ion battery according to the convective heat transfer coefficient were obtained for the 270 [°C] of constant temperature in the heating chamber, as shown in Figure 11. The graph ① in Figure 11 shows the thermal runaway characteristics in the case of 6 [W/(m^2·°C)] of the convective heat transfer coefficient, which is the minimum value in air condition, and it is known that the temperature of the battery was increased by 5 [°C] per minute and thermal runaway occurred in about 29 min. On the other hand, the graph ② in Figure 11 shows the thermal runaway

characteristics in the case of 15 [W/(m^2·°C)], which was made by forced ventilation of the battery module fan, and it was found that the temperature of the battery increased by 14.5 [°C] per minute and thermal runaway occurred in about 11 min. Namely, depending on the convective heat transfer coefficient, the temperature rise per minute was increased by about 9.5 [°C], and the time interval of thermal runaway was shortened by up to 18 min. Consequently, it is confirmed that as the convective heat transfer coefficient became higher due to the humidity and ventilation condition inside the battery module, the temperature of the battery rapidly rose and also thermal runaway occurred within a short time interval, and then thermal runaway from a single cell was easily able to propagate to adjacent cells depending on the convective heat transfer coefficients.

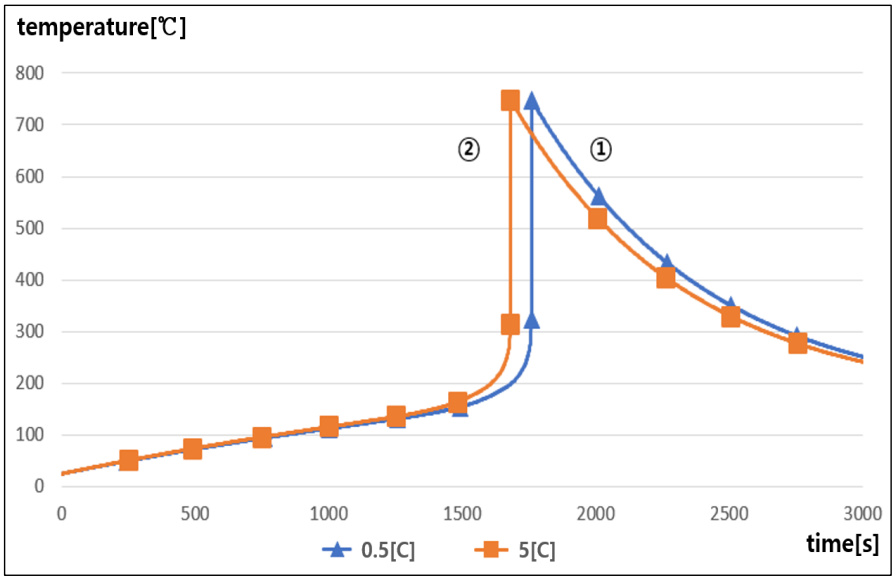

Figure 10. Profile of thermal runaway with the C-rate of charging and discharging.

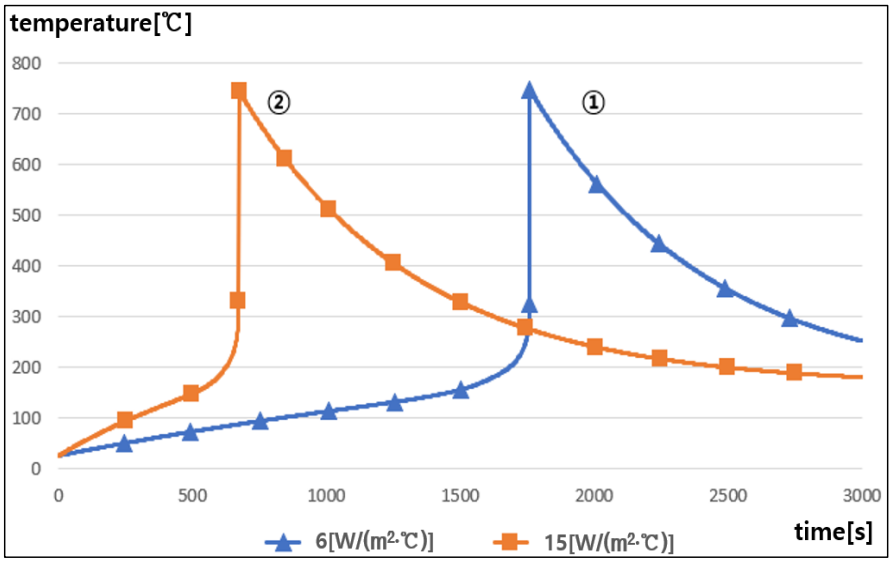

Figure 11. Profile of thermal runaway with the convective heat transfer coefficient.

5.6. Comprehensive Analysis

Based on the simulation results mentioned above, the processing characteristics of thermal runaway according to the operation conditions in ESSs such as the rising temperature rate, convective heat transfer coefficient, and C-rate of charging and discharging can be compared and summarized, as shown in Table 3. Based on the operation conditions, it is found that the rising temperature rate and the convective heat transfer coefficient were more critical in thermal runaway than the C-rate of charging and discharging. Therefore, in order to prevent thermal runaway in a Li-ion battery, it is necessary to install sensors monitoring the battery temperature and also cooling and ventilation systems that can cause suppression during the rapidly rising temperature. Also, an HVAC system should be applied to keep the optimal operation environment for ESSs.

Table 3. Occurrence time intervals of thermal runaway with the operation conditions in ESSs.

Operation Conditions		Occurrence Time Interval of Thermal Runaway [min]
Rising temperature rate [°C/min]	3	46
	5	28
	7	20
Convective heat transfer coefficient [W/(m^2·°C)]	6	29
	15	11
C-rate of charging and discharging [C]	0.5	29.33
	5	28

6. Conclusions

This paper has dealt with an evaluation modeling of thermal runaway using MATLAB/SIMULINK S/W based on the mathematical equations and it implemented the test device in order to evaluate the processing characteristics of thermal runaway according to operation conditions in ESSs. The main results of this paper are summarized as follows:

(1) It is confirmed that the proposed modeling is an effective and reliable tool to evaluate the processing characteristics of thermal runaway because the occurrence time intervals and maximum temperatures had almost the same values in both the test device and simulation modeling.
(2) It was found that as the rising temperature rate became higher, the chemical reaction inside the battery was accelerated and then the occurrence time interval of thermal runaway was shortened, and also, as the C-rate of charging and discharging became higher, the occurrence time interval of thermal runaway was slightly shortened due to the heat release from the internal resistance in the battery.
(3) It is confirmed that as the convective heat transfer coefficient became higher due to the humidity and ventilation condition inside the battery module, thermal runaway occurred within a short time interval, and then thermal runaway from a single cell can easily propagate to adjacent cells depending on the convective heat transfer coefficients.
(4) Based on the operation conditions in ESSs, it was found that the rising temperature rate and the convective heat transfer coefficient were more critical in thermal runaway than the C-rate of charging and discharging.

Author Contributions: All of the authors contributed to publishing this paper. M.-H.L., S.-M.C. and D.-S.R. carried out the test, modeling, and simulations, and they compiled the manuscript. The literature review and the simulation analysis were performed by K.-H.K., H.-S.Y. and S.-J.K., who also collected the data and investigated early works. All authors have read and agreed to the published version of the manuscript.

Funding: This research was supported by the Korea Institute of Energy Technology Evaluation and Planning (KETEP) grant funded by the Korean Government (MOTIE) (20224000000160, DC Grid Energy Innovation Research Center), and this research was supported the Korea Institute of Energy Technology Evaluation and Planning (KETEP) grant funded by the Korean Government (MOTIE) (RS-2024-00421994, Development of performance verification techniques and safety evaluation system for LiB-UPS System unit).

Data Availability Statement: The original contributions presented in the study are included in the article, further inquiries can be directed to the corresponding author.

Conflicts of Interest: The authors declare no conflicts of interest.

References

1. Nam, T.S. The here and the hereafter of Energy Storage System. *Trans. Korean Inst. Electr. Eng.* **2020**, *69*, 15–23.
2. Lim, S.Y.; Park, S.Y.; Yoo, S.H. The Economic Effects of the New and Renewable Energies Sector. *J. Energy Eng.* **2014**, *23*, 31–40. [CrossRef]
3. Park, K.M.; Kim, J.H.; Park, J.Y.; Bang, S.B. A Study on the Fire Risk of ESS through Fire Status and Field Investigation. *Fire Sci. Eng.* **2018**, *32*, 91–99. [CrossRef]
4. Lee, Y.B.; Kim, J.M.; Lee, M.H.; Rho, S.E.; Kim, S.J.; Rho, D.S. Safety Evaluation Method Considering Operation Environments and Applications in ESS. *Trans. Korean Inst. Electr. Eng.* **2024**, *73*, 773–783. [CrossRef]
5. Park, S.H.; Kang, J.G.; Kim, W.U.; Lim, H.W. A Study on Thermal Runaway Suppression Technology in Abnormal State for Energy Storage System(ESS) Using Lithium Secondary Battery. *J. Korean Inst. Illum. Electr. Install. Eng.* **2022**, *36*, 26–35.
6. Jang, H.J.; Song, T.S.; Kim, J.Y.; Kim, S.J.; Jang, T.H. Study on Analysis of Fire Factor and Development Direction of Standard/safety Requirement to Keep Safety for Energy Storage System (ESS). *Soc. Stand. Certif. Saf.* **2019**, *3*, 25–49. [CrossRef]
7. Jung, J.B.; Lim, M.G.; Kim, J.Y.; Rho, D.S. Characteristics of External Short-Circuit in Li-ion Battery Considering Operation and Environment Factors. *J. Korea Acad.-Ind. Coop. Soc.* **2021**, *22*, 663–672.
8. Lim, B.J.; Cho, S.H.; Lee, G.R.; Choi, S.M.; Park, C.D. Characteristics Analysis of Measurement Variables for Detecting Anomaly Signs of Thermal Runaway in Lithium-Ion Batteries. *Trans. Korean Hydrog. New Energy Soc.* **2022**, *33*, 85–94. [CrossRef]
9. *ANSI/CAN/UL 9540A(USA)*; Test Method for Evaluating Thermal Runaway Fire Propagation in Battery Energy Storage Systems. Sustainable Energy Action Committee: New York, NY, USA, 2019.
10. Peng, P.; Jiang, F. Thermal Safety of Lithium-ion Batteries with Various Cathode Materials: A Numerical Study. *Int. J. Heat Mass Transf.* **2016**, *103*, 1008–1016. [CrossRef]
11. Jiang, K.; Wang, T.; Li, X.; Duan, B.; Zhang, C. Simulation of Thermal Runaway Prediction Model for Nickel-rich Lithium ion Batteries. In Proceedings of the Chinese Automation Congress, Jinan, China, 20–22 October 2017; pp. 1293–1297.
12. An, Z.; Shah, K.; Jia, L.; Ma, Y. Modeling and Analysis of Thermal Runaway in Li-ion Cell. *Appl. Therm. Eng.* **2019**, *160*, 113960. [CrossRef]
13. Ren, D.; Feng, X.; Lu, L.; Ouyang, M.; Zheng, S.; Li, J.; He, X. An Electrochemical-thermal Coupled Overcharge-to-thermal-runaway Model for Lithium Ion Battery. *J. Power Sources* **2017**, *364*, 328–340. [CrossRef]
14. Liu, H.; Wei, Z.; He, W.; Zhao, J. Thermal issues about Li-ion batteries and recent progress in battery thermal management systems: A review. *Energy Convers. Manag.* **2017**, *150*, 304–330. [CrossRef]
15. Coman, P.T.; Darcy, E.C.; Veje, C.T.; White, R.E. Modelling Li-Ion Cell Thermal Runaway Triggered by an Internal Short Circuit Device Using an Efficiency Factor and Arrhenius Formulations. *J. Electrochem. Soc.* **2017**, *164*, 587–593. [CrossRef]
16. MacNeil, D.D.; Dahn, J.R. Test of Reaction Kinetics Using Both Differential Scanning and Accelerating Rate Calorimetries As Applied to the Reaction of Li_xCoO_2 in Non-aqueous Electrolyte. *Am. Chem. Soc.* **2001**, *105*, 4430–4439. [CrossRef]
17. Abada, S.; Marlair, G.; Lecocq, A.; Petit, M.; Sauvant-Moynot, V.; Huet, F. Safety focused modeling of lithium-ion batteries: A review. *J. Power Sources* **2016**, *306*, 178–192. [CrossRef]
18. Li, J.; Lotfi, N.; Landers, R.G.; Park, J. A Single Particle Model for Lithium-Ion Batteries with Electrolyte and Stress-Enhanced Diffusion Physics. *J. Electrochem. Soc.* **2017**, *164*, 874–883. [CrossRef]
19. Guduru, A.; Northrop, P.W.; Jain, S.; Crothers, A.C.; Marchant, T.R.; Subramanian, V.R. Analytical solution for electrolyte concentration distribution in lithium-ion batteries. *J. Appl. Electrochem.* **2012**, *42*, 189–199. [CrossRef]
20. Baba, N.; Yoshida, H.; Nagaoka, M.; Okuda, C.; Kawauchi, S. Numerical simulation of thermal behavior of lithium-ion secondary batteries using the enhanced single particle model. *J. Power Sources* **2014**, *252*, 214–228. [CrossRef]
21. An, Z.; Jia, L.; Wei, L.; Dang, C.; Peng, Q. Investigation on Lithium-ion Battery Electrochemical and Thermal Characteristic Based on Electrochemical-thermal Coupled Model. *Appl. Therm. Eng.* **2018**, *137*, 792–807. [CrossRef]
22. Hwang, S.Y.; Choi, S.M.; Jian, S.; Choi, H.S.; Rh, D.S. A Study on the Detection Algorithm of Off-gas to Prevent Thermal runaway of Li-ion Battery for ESS. *Trans. Korean Inst. Electr. Eng.* **2022**, *71*, 1787–1795. [CrossRef]
23. Kim, G.H.; Pesaran, A.; Spotnitz, R. A Three-dimensional Thermal Abuse Model for Lithium-ion Cells. *J. Power Sources* **2007**, *170*, 476–489. [CrossRef]

24. Wang, H.; Du, Z.; Rui, X.; Wang, S.; Jin, C.; He, L.; Zhang, F.; Wang, Q.; Feng, X. A Comparative Analysis on Thermal Runaway Behavior of Li ($Ni_xCo_yMn_z$) O_2 Battery with Different Nickel Contents at Cell and Module Level. *J. Hazard. Mater.* **2020**, *393*, 122361. [CrossRef] [PubMed]
25. *IEC 62619:2022*; Secondary Cells and Batteries Containing Alkaline or Other Non-Acid Electrolytes—Safety Requirements for Secondary Lithium Cells and Batteries, for Use in Industrial Applications. International Electrotechnical Commission: Geneva, Switzerland, 2022.